# Rashba Effect in the Tl-induced (1×1) and (3×1) Structures on Ge(111)

The electronic structure and spin splitting caused by the Rashba spin-orbit (SO) coupling were investigated for the (1×1) and (3×1) structures on the Tl/Ge(111) surface by angle-resolved photoelectron spectroscopy (ARPES) and a first-principles band calculation. In the calculations with the SO interaction taken into account, the surface states with Tl 6p character show spin splitting. While the corresponding states were observed by ARPES, the spin splitting could not be confirmed due to the limited energy resolution. The largest splitting of ~700 meV is found for the lowest unoccupied states on the (1×1) surface. The wavefunction amplitude of the spin-split states is concentrated at the level of Tl, indicating that the heavy core potential of Tl is important for a large Rashba effect.

The Rashba spin-orbit (SO) interaction in two-dimensional electron systems has become a hot topic in both surface and semiconductor science in recent years. The SO interaction originates from the potential gradient normal to the surface ($\vec{\nabla}V$) and is described by $H = \frac{\hbar}{4m_e^2c^2}\vec{\sigma}\cdot(\vec{\nabla}V\times\vec{p})$ [1,2] for two-dimensional free electrons, where $\vec{\sigma}$ and $\vec{p}$ are the Pauli spin operator and the electron momentum, respectively. The SO interaction causes spin-split states on a non-magnetic substrate without an external magnetic field, which could provide an important advantage for future applications in spintronics. The Rashba spin splitting in surface states was first observed on Au(111) [3]. A larger splitting, of the order of 1 eV was observed for both low-index Bi surfaces and Bi-induced structures on Ag surfaces [4-6]. The free-electron model cannot explain these large splittings, and the heavy core potential is considered to be important for understanding the spin splitting in surface states. In order to investigate the SO interaction on a semiconductor surface, we studied Tl-induced (1×1) and (3×1) structures on Ge(111) substrate by using angle-resolved photoelectron spectroscopy (ARPES) and a first-principles band calculation [7, 8]. On the (1×1) surface, Tl atoms are located at $T_4$ sites on bulk-truncated Ge(111) (Fig. 1(a)). The (3×1) surface has a honeycomb-chain-channel structure, the common framework for alkali-metal-induced (3×1) structures on Si(111) and Ge(111), with Tl residing on $H_3$ sites (Fig. 1(b)).
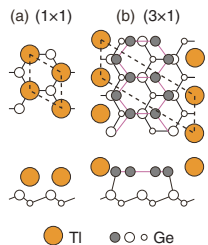


Figure 1
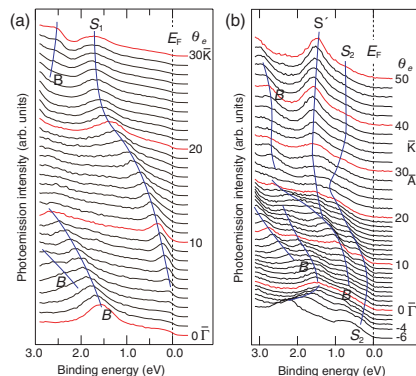Atomic structure models of the (1×1) and (3×1) structures on Tl/Ge(111).



Figure 2
ARPES spectra of (a) Tl/Ge(111)-(1×1) along ΓK with hν=21.2 eV [6] and (b) Tl/Ge(111)-(3×1) along ΓA with hν=16 eV [7].

We carried out the ARPES experiments at BL-18A using photon energies hν=12, 16, 22, 40 eV, and at Kyoto University using hν=21.2 eV. The first-principles band calculation incorporating the SO interaction was performed with the WIEN2k computer code.

Figures 2 show ARPES spectra of the (1×1) and (3×1) structures. A Tl-induced bands $S_1$ and $S_2$ are found in the bulk-band gap on the respective surfaces. Figure 3(a) shows the calculated band structure of the (1×1) structure. The surface band structure is characterized by $S_1$, the dangling-bond state on the topmost Ge, and $U_1$, the Tl–Tl anti-bonding state. Although $U_1$ is partially occupied in the calculation with limited k-point sampling, the corresponding feature was not observed in ARPES. Tl interacts with Ge(111) as a monovalent ion due to the inert-pair effect, and the Tl–Ge bond has a strong ionic character. Similar behavior of Tl is also seen on the (3×1) structure. The charge transfer from Tl to Ge terminates the dangling bonds of the honeycomb chain Ge adatoms. The $S_2$ band in Fig. 3(b) is mainly derived from the dangling-bond state of the Ge adatom facing Tl.
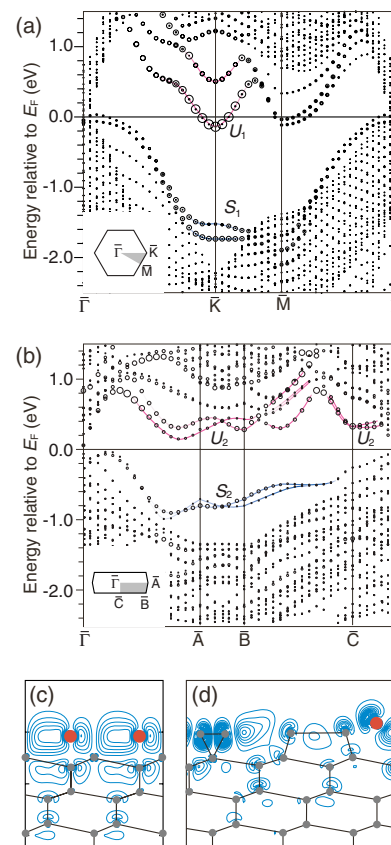


Figure 3
Calculated band structure of (a) the (1×1) and (b) the (3×1) structures on Tl/Ge(111). Also shown are the wavefunctions of (c) $U_1$ and (d) $U_2$ at $\bar{K}$ and $\bar{A}$, respectively.

The calculated surface bands show spin splittings of up to 150–700 meV. The calculated $S_1$ band shows a spin splitting of ~200 meV at around $\bar{K}$, which is probably responsible for the broadening of the $S_1$ feature from $\bar{\Gamma}$ to $\bar{K}$ in Fig. 2(a). As to $S_2$ and $U_2$, it is worth noting that the spin splitting of $U_2$ disappears at the middle of $\bar{A}-\bar{B}$ and $\bar{C}$. This behavior is consistent with the inhibition rule of the spin splitting due to the Rashba SO coupling. The splittings of $U_1$ and $U_2$ are relatively larger than those of $S_1$ and $S_2$. This difference is ascribed to the stronger Tl 6p character of $U_1$ and $U_2$. Figures 3(c) and (d) show the wavefunction distributions of the $U_1$ and $U_2$ states at $\bar{K}$ and $\bar{A}$, respectively. The states at $\bar{K}$ with the largest splitting of ~700 meV have purely Tl $6p_x+6p_y$ character and are strongly localized at the Tl layer.

In conclusion, we found on Tl/Ge(111) large spin splittings of the surface states due to the Rashba SO coupling. The dominant Tl 6p contribution to the lowest unoccupied states causes the large spin splittings.

## REFERENCES
[1] E.I. Rashba, *Sov. Phys. Sol. St.*, **2** (1960) 1109.
[2] Y.A. Bychkov and E.I. Rashba, *JETP Lett.*, **39** (1984) 78.
[3] S. LaShell, B.A. McDougall and E. Jensen, *Phys. Rev. Lett.*, **77** (1996) 3419.
[4] Yu.M. Koroteev, G. Bihlmayer, J.E. Gayone, E.V. Chulkov, S. Blügel, P.M. Echenique and Ph. Hofmann, *Phys. Rev. Lett.*, **93** (2004) 046403.
[5] C.R. Ast, J. Henk, A. Ernst, L. Moreschini, M.C. Falub, D. Pacilé, P. Bruno, K. Kern and M. Grioni, *Phys. Rev. Lett.*, **98** (2007) 186807.
[6] T. Nakagawa, O. Ohgami, Y. Saito, H. Okuyama, M. Nishijima and T. Aruga, *Phys. Rev. B*, **75** (2007) 155409.
[7] S. Hatta, C. Kato, N. Tsuboi, S. Takahashi, H. Okuyama, T. Aruga, A. Harasawa, T. Okuda and T. Kinoshita, *Phys. Rev. B*, **76** (2007) 075427.
[8] S. Hatta, T. Aruga, C. Kato, S. Takahashi, H. Okuyama, A. Harasawa, T. Okuda and T. Kinoshita, *Phys. Rev. B*, **77** (2008) 245436.

## BEAMLINE
18A

**S. Hatta[1,2], C. Kato[1], S. Takahashi[1], A. Harasawa[3], T. Okuda[3], T. Kinoshita[3], H. Okuyama[1] and T. Aruga[1,2] ([1]Kyoto Univ., [2]JST CREST, [3]The Univ. of Tokyo)**

# An *In Situ* Photoemission Study of Pr$_{1-x}$Ca$_x$MnO$_3$ Epitaxial Thin Films with Suppressed Charge Ordering

We have performed an *in situ* photoemission study of Pr$_{1-x}$Ca$_x$MnO$_3$ thin films grown on LaAlO$_3$ (001) substrates and observed the effect of epitaxial strain on the electronic structure. The band dispersions determined by angle-resolved photoemission spectroscopy showed that the films were insulators. The dispersions could not be explained by the metallic band structure of the C-type anti-ferromagnetic state, where spins are coupled antiferromagnetically within the plane and ferromagnetically along the chain, due to localization of electrons along the ferromagnetic chain direction or due to another type of spin-orbital ordering. We observed a doping-induced chemical-potential shift toward the Fermi level ($E_F$) with hole doping, but no spectral weight transfer near $E_F$. These results can be explained by the suppression of charge ordering and charge fluctuations due to compressive strain from the substrate.

Hole-doped perovskite manganese oxides R$_{1-x}$A$_x$MnO$_3$, where R is a rare-earth (R = La, Nd, Pr) and A is an alkaline-earth atom (A = Sr, Ba, Ca), have attracted much attention because of their remarkable physical properties such as colossal magnetoresistance and ordering of spin, charge, and orbitals [1]. Most of the half-doped manganites (x = 0.5) with small bandwidths exhibit the so-called "CE-type" anti-ferromagnetic (AF) charge ordering (CO), with alternating Mn$^{3+}$ and Mn$^{4+}$ states within the (001) plane in the form of stripes [2]. Pr$_{1-x}$Ca$_x$MnO$_3$ (PCMO), which has the narrowest bandwidth, has a particularly stable CO state with a wide hole concentration range between x = 0.3 and 0.75 [3]. In this work, we have used photoemission spectroscopy to study the electronic structure of PCMO thin films grown on LaAlO$_3$ (LAO) substrates [4]. The substrates create a compressive strain on the films, which is expected to suppress CO and charge fluctuations [5].

Epitaxial thin films of PCMO with thicknesses of about 40 nm were fabricated using the pulsed laser deposition method. Single crystals of LAO (001) were used as the substrates. The in-plane lattice constants of the PCMO thin films were the same as those of LAO (a = 3.792 Å), confirming epitaxial and coherent growth of the thin films on the substrates. For all compositions, the out-of-plane lattice constants were longer than the in-plane lattice constants, indicating that the PCMO thin films were under compressive strain. The photoemission measurements were performed at BL-1C and 2C, using a combined laser molecular-beam epitaxy and photoemission spectrometer system [6]. The photoemission spectra were recorded using a Gammadata Scienta SES-100 spectrometer with the total energy resolution set to about 150 - 400 meV depending on photon energy. All spectra were recorded at room temperature, except for the angle-resolved photoemission spectroscopy (ARPES) measurements which were performed at 20 K.

Figure 1 shows the normal-emission ARPES spectra (out-of-plane band dispersions) of PCMO (x=0.4) (a), and tight-binding band-structure calculations of the previously proposed C-type AF state (b). The strong dispersion of the Mn 3d e$_g$ bands predicted by the calculation (enclosed by a blue rectangle in Fig. 1 (b)) was not observed in the experiment. The e$_g$ electrons appear to be localized along the ferromagnetic chain direction due to disorder and/or electron correlation. In the valence band, we observed an energy shift of the spectra which is attributed to the effect of the chemical-potential shift. No new states appeared near the Fermi level ($E_F$) due to hole doping. This result is in contrast with the results for bulk PCMO, where spectral weight transfer from high to low energies occurs near $E_F$ due to hole doping [7]. From the present results, we conclude that our PCMO thin films were good insulators with no dynamical "phase separation." The suppression of incommensurate charge fluctuations is due to the compressive strain effects from the LAO substrates. This difference in electronic structure between the bulk and thin film samples is shown schematically in Fig. 2. In the bulk samples, there is a macroscopic and/or microscopic (one-dimensional stripe type) phase separation, but in the thin film samples with in-plane compressive strain, PCMO behaves as a homogeneous complete insulator.
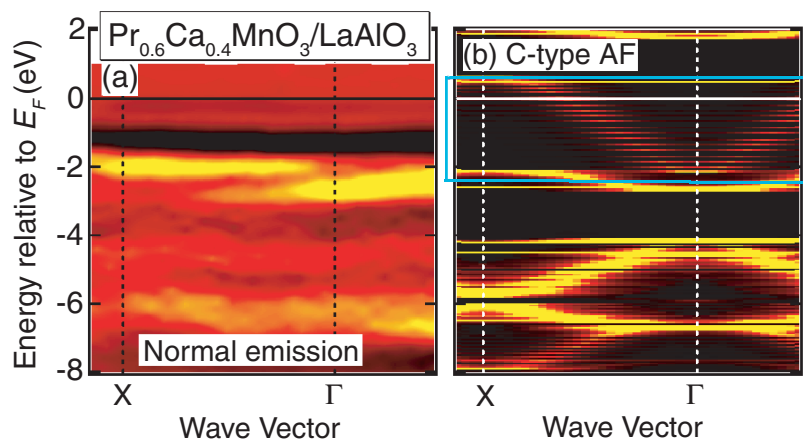


Figure 1
Comparison of the ARPES spectra measured in normal-emission geometry with a tight-binding band structure calculation. The bright parts correspond to energy bands. (a) Experimental band structure of PCMO (x = 0.4). (b) Tight-binding calculation of the C-type AF state.



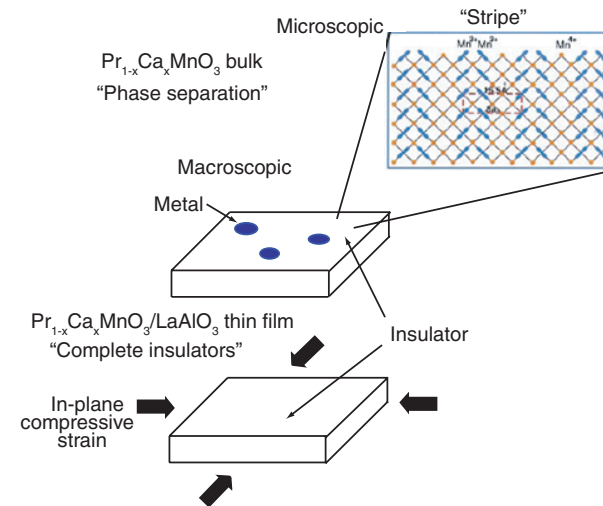Figure 2
Schematic illustration of the electronic structures of PCMO for bulk and thin film samples.

**REFERENCES**
[1] Y. Tokura and N. Nagaosa, *Science*, **288** (2000) 462.
[2] Z. Jirak, S. Krupicka, V. Nekvasil, E. Pollert, G. Villeneuve and F. Zounova, *J. Magn. Magn. Mater.*, **15** (1980) 519.
[3] Y. Tomioka, A. Asamitsu, H. Kuwahara, Y. Moritomo and Y. Tokura, *Phys. Rev. B*, **53** (1996) 1689.
[4] H. Wadati, A. Maniwa, A. Chikamatsu, I. Ohkubo, H. Kumigashira, M. Oshima, A. Fujimori, M. Lippmaa, M. Kawasaki and H. Koinuma, *Phys. Rev. Lett.*, **100** (2008) 026402.
[5] Z.Q. Yang, Y.Q. Zhang, J. Aarts, M.-Y. Wu and H.W. Zandbergen, *Appl. Phys. Lett.*, **88** (2006) 072507.
[6] K. Horiba, H. Ohguchi, H. Kumigashira, M. Oshima, K. Ono, N. Nakagawa, M. Lippmaa, M. Kawasaki and H. Koinuma, *Rev. Sci. Instrum.*, **74** (2003) 3406.
[7] K. Ebata, H. Wadati, M. Takizawa, A. Fujimori, A. Chikamatsu, H. Kumigashira, M. Oshima, Y. Tomioka and Y. Tokura, *Phys. Rev. B*, **74** (2006) 064419.

H. Wadati[1, 2], A. Maniwa[1], A. Chikamatsu[1], I. Ohkubo[1], H. Kumigashira[1, 3], M. Oshima[1, 3], A. Fujimori[1], M. Lippmaa[4], M. Kawasaki[3, 5] and H. Koinuma[1, 6] ([1]Univ. of Tokyo, [2]UBC, [3]CREST-JST, [4]ISSP, [5]Tohoku Univ., [6]NIMS)

# Estimate of the Time Constant for Proton Transfer between Water and Hydroxyl on a Pt(111) Surface

The time scale of proton transfer between $H_2O$ and OH on a Pt(111) surface was measured using a combination of laser-induced thermal desorption (LITD) and micro-scale X-ray photoelectron spectroscopy (micro-XPS). A one-dimensional patterned distribution OH + $H_2O$/$H_2O$/OH + $H_2O$ was initially prepared on the Pt(111) surface by LITD, and the time evolution of the spatial distribution of OH and $H_2O$ was measured using micro-XPS. From quantitative analyses based on a diffusion equation, we found two proton-transfer pathways with time constants at 140 K of 5.2 ± 0.9 ns and 48 ± 12 ns. The two pathways were respectively attributed to direct proton transfer to the neighboring site, and $H_3O^+$-mediated transfer to the next-nearest site.

Proton transfer in hydrogen-bonded systems is a fundamental natural process and plays a significant role in many physical, chemical, and biological processes. Knowledge of the time scale on which the proton transfer occurs is essential for the understanding of these processes, although it is not always straightforward to determine the transfer rate experimentally. On a Pt(111) surface, OH and $H_2O$ molecules form a well-ordered two-dimensional (2D) mixed honeycomb structure. The OH + $H_2O$ mixed phase has previously been observed during water formation from oxygen and hydrogen on a Pt(111) surface [1], and it has been suggested that proton transfer in the mixed phase plays a crucial role in promoting the autocatalytic reaction [2]. Proton transfer in the mixed structure was also suggested by studies using density functional theory [3] and infrared absorption reflection spectroscopy [4]. However the time scale of the proton transfer in this 2D hydrogen-bonding network was until now unknown. In this work we have estimated experimentally the time scale of the proton transfer from $H_2O$ to OH in the mixed phase on a Pt(111) surface [5].

The experiments were performed at BL-7A under ultrahigh vacuum conditions. As shown in Fig. 1(a), a one-dimensional (1D) spatial distribution OH+$H_2O$/$H_2O$/OH+$H_2O$ was prepared by scanning a pulsed Nd:YAG laser beam along one direction on the mixed OH + $H_2O$ overlayer to make a 400 μm wide 1D vacant band, with subsequent filling of the vacant area by $H_2O$ molecules. The coverage distribution changes of OH and $H_2O$ were monitored using micro-XPS with a spatial resolution of 16.5 μm at 140 K.

Figure 1(b) shows the micro-XPS image obtained for the initial distribution. The coverage distributions for OH and $H_2O$ were determined at different elapsed times by fitting to standard spectra, the results of which are shown in the top part of Fig. 2. In the central region, OH coverage increases over time while $H_2O$ coverage decreases. Because OH does not diffuse at 140 K [1], it can be deduced that the OH observed in the central region results from proton transfer between $H_2O$ and OH.
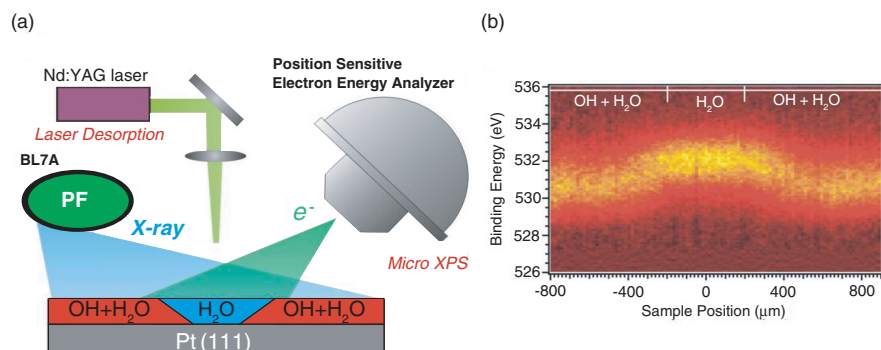


Figure 1
(a) Schematic of the experimental setup for studying proton transfer in a mixed OH+$H_2O$ overlayer on a Pt(111) surface. The 1D patterned distribution OH+$H_2O$/$H_2O$/OH+$H_2O$ on Pt(111) was prepared by laser induced thermal desorption, and the changes of coverage distribution was measured by a micro-XPS technique. (b) XPS spectra obtained from the initial distribution of the 1D modulated structures. The horizontal and vertical axes of the image correspond to the surface position and the binding energy of the XPS spectra, respectively.
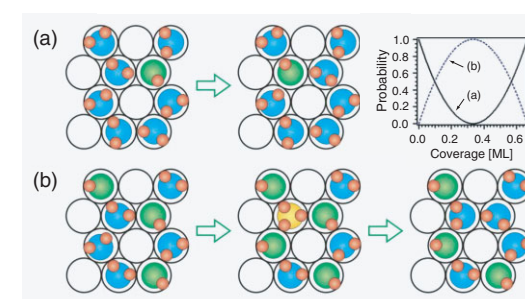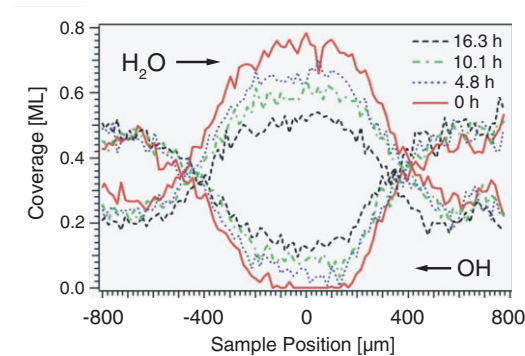


Figure 2
(Top) Coverage distributions of OH and $H_2O$ at the 1D patterned structure at different elapsed times. (Bottom) Schematics of the two proton transfer processes: (a) simple proton transfer and (b) proton transfer via $H_3O^+$. The probabilities of the two processes are shown as a function of the coverage.

From the observed distribution changes, we estimated the rate of proton transfer based on a diffusion equation considering two pathways. The first process is simple proton transfer from $H_2O$ to a neighboring OH, as shown in Fig. 2(a). The second process is $H_3O^+$-mediated proton transfer, as shown in Fig. 2(b). From fitting analyses using the diffusion equation, the time constant of the simple proton transfer process was found to be 5.2 ± 0.9 ns, and that of the $H_3O^+$-mediated process to be 48 ± 12 ns. These time constants are intermediate to those which occur for liquid and 3D-solid phases, which relates to the degrees of freedom available for proton transfer. We also checked for any solvent effects on the 2D proton transfer by performing spatio-temporal tracing of the OH+$H_2O$/$H_2O$/OH+$H_2O$ overlayer under water multilayers at 140 K, and observed a significant reduction in proton transfer rate in the 2D hydrogen-bonding network. This suggests peripatetic behavior of the protons, with transfer to $H_2O$ molecules in the upper layer. The understanding of proton dynamics at 2D interfaces will be important for understanding protonics at interfaces such as fuel-cell electrodes and biological membranes.

## REFERENCES
[1] C. Sachs, M. Hildebrand, S. Völkening, J. Wintterlin and G. Ertl, *Sience*, **293** (2001) 1635.
[2] M. Nagasaka, H. Kondoh and T. Ohta, *J. Chem. Phys.*, **122** (2005) 204704.
[3] A. Michaelides and P. Hu, *J. Am. Chem. Soc.*, **123** (2001) 4235.
[4] C. Clay, S. Haq and A. Hodgson, *Phys. Rev. Lett.*, **92** (2004) 046102.
[5] M. Nagasaka, H. Kondoh, K. Amemiya, T. Ohta and Y. Iwasawa, *Phys. Rev. Lett.*, **100** (2008) 106101.

## BEAMLINE
7A

**M. Nagasaka[1,2], H. Kondoh[1,3], K. Amemiya[1,4], T. Ohta[1,5] and Y. Iwasawa[1]** ([1]The Univ. of Tokyo, [2]IMS, [3]Keio Univ., [4]KEK-PF, [5]Ritsumeikan Univ.)

# CO Adsorption Effects on the Magnetism of Fe/Cu(001) Thin Films

CO adsorption effects on the magnetism of Fe films on Cu(001) were studied at 100 K as a function of film thickness. It was found that CO adsorption does not affect the magnetic properties of a 2 ML Fe film, but induces spin reorientation from out-of-plane to in-plane magnetization for 3 and 4 ML films. It also causes a decrease in overall magnetization, which can be attributed to a reduction in surface magnetization. Possible origins of these complicated magnetic behaviors are discussed.

The atomic and magnetic properties of Fe thin films on Cu(001) have been extensively studied as prototypical cases of magnetic thin films[1]. Fe/Cu(001) films exhibit three characteristic regimes; regimes I (< 4 ML), II (5-11 ML), and III (> 12 ML). Here we focus on regime I, which exhibits a distorted fcc structure and a ferromagnetic coupling throughout the whole film with perpendicular magnetization.

In this article, we report on the effects of CO adsorption on the magnetism of Fe/Cu(001) films [2]. Films with 2 ML Fe are not affected, but 4 ML films show drastically changed magnetic properties following adsorption, with the direction of magnetization rotating from perpendicular to in-plane, and the two surface layers losing their spin magnetic moment.

The experiments were performed at BL-7A and BL-11A, which are equipped with an ultrahigh vacuum chamber. Fe/Cu(001) films were prepared in the chamber at room temperature. Conventional and depth-resolved X-ray magnetic circular dichroism (XMCD) measurements [3] were carried out at 100 K with normal (90°) and grazing (30°) X-ray incidence, hereafter referred to as "NI" and "GI". After measurements of the bare films, each film was dosed with 5 L of CO and the measurements repeated.

The Fe $L$-edge XMCD spectra of Fe(2 and 4 ML)/Cu(001) are shown in Figs. 1(a) and (c). The spectra are quite similar, revealing perpendicular magnetization with spin magnetic moments of about $m_s = 2.4$ $\mu_B$ for both films.

Next we discuss the effects of CO adsorption on the films. Fe $L$-edge XMCD spectra of CO-adsorbed 2 and 4 ML Fe films are shown in Figs. 1 (b) and (d). The XMCD spectra of CO/Fe(2 ML)/Cu(001) are essentially the same as those of Fe(2 ML)/Cu(001): CO adsorption does not affect the XMCD spectra of the 2 ML Fe film. In contrast, the XMCD spectra of CO/Fe(4 ML)/Cu(001) exhibit almost no signal for NI geometry, with significant signal only for GI geometry. These features directly indicate the in-plane magnetization of the film. Thus it can be concluded that CO adsorption rotates the easy axis of magnetization of the 4 ML film from perpendicular to in-plane.
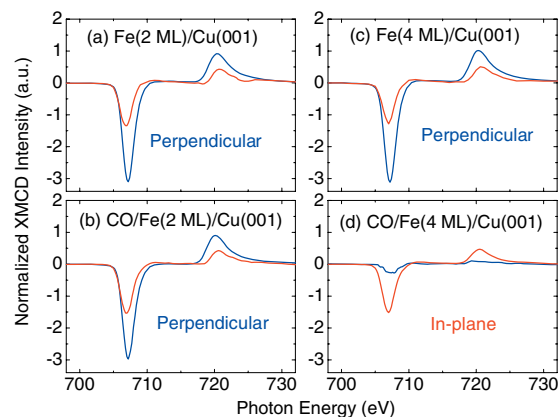


Figure 1
Fe $L$-edge XMCD spectra of the 2 ML Fe film before (a) and after (b) CO adsorption. The same spectra for the 4 ML Fe film are shown in (c) and (d). The blue spectra represent XMCD spectra for NI geometry and the red spectra those for GI geometry.
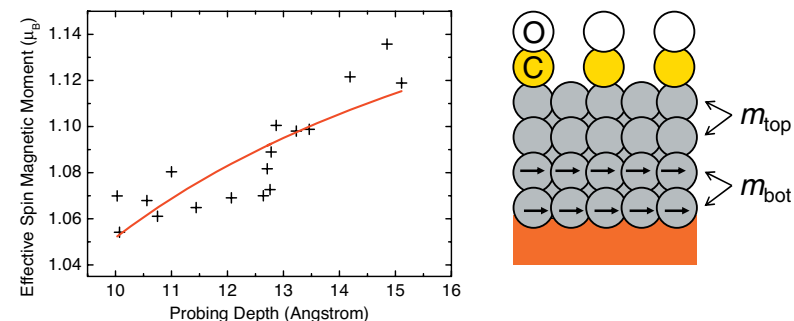


Figure 2
Probing depth dependence of the Fe effective spin magnetic moment, $m_s$, of CO/Fe(4 ML)/Cu(001), along with the schematic model. The crosses represent experimentally obtained moments, and the solid red line a fit with $(m_{top}, m_{bot}) = (0.17, 2.31)$ $\mu_B$.

The spin magnetic moment obtained for CO/Fe(4 ML)/Cu(001) of $1.1 \mu_B$ is about half the magnitude of that of CO/Fe(2 ML)/Cu(001) (2.3 $\mu_B$). This apparent decrease in $m_s$ is considered to be due to the disappearance of the contributions to $m_s$ of the top two layers. The depth-resolved XMCD spectra give us the probing depth (effective electron escape depth) dependence of $m_s$, shown in Fig. 2. The spin magnetic moment decreases with decreasing probe depth, directly showing that the moment is small near the surface. The plot shown in Fig. 2 was analyzed with a simple model, composed of the top two layers and bottom two layers, also shown in Fig. 2. The top two layers have little magnetic moment (0.17 $\mu_B$), while the bottom two layers exhibit a moment of 2.31 $\mu_B$.

In summary, the effects of CO adsorption on the magnetism of Fe(2 and 4 ML)/Cu(001) were studied at 100 K. The 2 ML film was not affected by CO adsorption. In contrast, the 4 ML Fe films changed their magnetism drastically, with the direction of magnetization rotating from perpendicular to in-plane. In addition, the two surface layers lose their spin magnetic moment upon CO adsorption, and consequently the bottom two layers show magnetization. These complex magnetic phases can be interpreted by assuming that CO adsorption kills the ferromagnetic coupling of the surface layers while the Cu(001) substrate always maintains ferromagnetic coupling with the adjacent two layers.

## REFERENCES
[1] W.L. O'Brien, T. Droubay and B.P. Tonner, *Phys. Rev. B,* (1996) **54** 9297.
[2] H. Abe, K. Amemiya, D. Matsumura, J. Miyawaki, E.O. Sako, T. Ohtsuki, E. Sakai and T. Ohta, *Phys. Rev. B,* (2008) **77** 054409.
[3] K. Amemiya, S. Kitagawa, D. Matsumura, H. Abe, T. Ohta and T. Yokoyama, *Appl. Phys. Lett.*, **84**, (2004) 936.
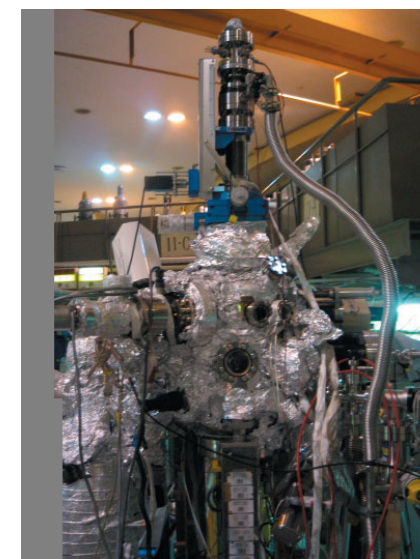
**H. Abe[1], K. Amemiya[2], D. Matsumura[3], J. Miyawaki[4], E.O. Sako[2], T. Ohtsuki[5], E. Sakai[5] and T. Ohta[6] ([1]Keio Univ., [2]KEK-PF, [3]JAEA, [4]Riken Harima Inst., [5]The Univ. of Tokyo, [6]SR Center, Ritsumeikan Univ.)**